COMMUNICATIONS: SIF Congress 2022

Time-resolved core level photoemission reveals transient lattice distortions in 2H-MoTe$_2$ crystals(*)

R. Costantini[1][2]

[1] *Dipartimento di Fisica, Università di Trieste - Via Valerio 2, 34127 Trieste, Italy*
[2] *CNR-IOM - Strada Statale 14, km 163.5, 34149 Trieste, Italy*

Summary. — Time-resolved X-ray photoemission has been used to investigate the photo-induced lattice dynamics in a 2H-MoTe$_2$ crystal. Two different effects are present at long and short timescales: in the microsecond range, core level shifts due to the surface photovoltage fields are detected; in the sub-nanosecond range, a shift in the opposite direction is observed, indicating that its origin may be due to a different physical process. With the support of theoretical calculations, it is shown that the latter energy shift can be ascribed to a transient lattice deformation, with a measured lifetime in the order of $\sim$600 ps.

1. – Introduction

The study of the photo-excitation dynamics of organic films and hybrid organic-inorganic heterojunctions has become a topic of great relevance for the development of new, highly efficient optoelectronic devices [1-3]. Such task represents an important step towards a more environmentally sustainable production, storage and use of energy, with the ultimate goal of cutting CO_2 emissions.

Transition metal dichalcogenides (TMDs) are a class of materials that are particularly suitable for designing innovative devices. TMDs are layered materials with a MX$_2$ stoichiometry, in which the transition metal atoms (M) are sandwiched between two chalcogen layers (X = S, Se, Te). The numerous combinations of M and X elements translates into a broad spectrum of electronic properties, which also depend on the crystal phase and on the thickness of the material [4]. Different TMD polytypes correspond to a different character: the trigonal prismatic ($1H/2H$) phase is semiconducting, while the

---

octahedral ($1T/1T'$) structure is (semi-)metallic. In addition, thinning a semiconducting TMD to a single layer causes its indirect gap to become direct.

Molybdenum ditelluride ($MoTe_2$) is a TMD that is particularly interesting from a technological point of view. In its $2H$ phase it has a bandgap in the near infrared region (0.9 eV in the bulk and 1.1 eV in the monolayer), making it a viable alternative to silicon in optoelectronic devices. Moreover, carrier multiplication has been demonstrated in 2H-$MoTe_2$ [5], implying potential advantages in light harvesting applications. $MoTe_2$ can also be found in the $1T'$ phase, which is metastable; a barrier of around 0.7 eV [6,7] prevents the transition from $1T'$ to the $2H$ phase. This property has been cleverly exploited to draw metallic patterns in a semiconducting $2H$ substrate via laser excitation, to create an ohmic heterophase homojunction [8]: such result highlights the importance of gaining in-depth knowledge and control of the photo-induced phase transitions in TMDs. Multiple studies have addressed the photoexcited carrier dynamics in $2H$-$MoTe_2$ [9-13], showing evidence that the lattice cooling occurs in the 100 ps timescale. With a theoretical analysis, Peng and co-workers have shown that the photo-induced $2H$-$1T'$ transition in $MoTe_2$ occurs via a purely electronic excitation, which softens the A'_2 phononic mode [14].

In this work, the structural dynamics of optically excited 2H-$MoTe_2$ are investigated by means of time-resolved X-ray photoemission spectroscopy (tr-XPS). These measurements are performed using 515 nm laser pulses to optically excite the TMD crystal, and X-ray pulses from the Elettra synchrotron as a probe. Two different effects are observed: at delay times in the microsecond range, the binding energies of the photoemission peaks shift to lower binding energies, as compared to the unpumped sample; at delays in the sub-nanosecond range, the measured core levels shift to higher binding energies. The former effect is ascribed to the formation of long-lived surface photovoltage, while the latter must have a different nature. With the support of density functional theory (DFT) calculations, the positive binding energy shift was related to the lattice deformation of $MoTe_2$ along the A'_2 mode, in which Mo and Te atoms are displaced in opposite out-of-plane directions. These results illustrate how tr-XPS, supported by DFT calculations, may probe transient lattice deformations, therefore expanding the tool set for the characterization of phase transitions in TMDs.

2. – Experimental

The 2H-$MoTe_2$ crystal (>99.995%purity) was purchased from HQ Graphene and cleaved in ultra-high vacuum ($<3 \times 10^{-10}$ mbar). Time-resolved photoemission measurements were performed at the ANCHOR-SUNDYN endstation of the ALOISA beamline at the Elettra synchrotron in Trieste [15]. The second harmonic (2.4 eV, 515 nm) of an Yb-doped yttrium aluminum garnet (Yb:YAG) fiber laser (Tangerine HP, Amplitude Systèmes) was used to optically excite the samples. Static XPS spectra in the pump on/pump off series were acquired with a photon energy of 400 eV and a pass energy of 20 eV. In these measurements, the use of the multibunch synchrotron radiation allows detecting long-lived effects (microsecond scale) with a high signal-to-noise ratio, as previously reported on organic heterojunctions [16]. The reversibility of the effect and the absence of radiation damage were ensured by recording the spectra in pump off/pump on sequences.

Instead, to measure the time-resolved X-ray photoemission, hybrid pulses of the Elettra storage ring were used as a probe; the laser was synchronized to excite one every three X-ray pulses, allowing for the acquisition of both a pumped and an unpumped pulse in the same acquisition window, as detailed in ref. [17]. The temporal overlap between the

pump and probe pulses was calibrated by measuring the surface photovoltage shift on a silicon crystal. Due to the significantly longer pulse duration of the synchrotron compared to the laser, $\sim$100 ps and $\sim$300 fs, respectively, the temporal resolution in time-resolved XPS on this setup is limited by the former, and was measured to be 120 ps.

3. – Results and discussion

In order to verify the damage threshold of the 2H-MoTe$_2$ crystal prior to the time-resolved measurements, a series of photoemission spectra of the Mo and Te core levels were acquired while illuminating the sample with 2.4 eV laser radiation at increasing fluences. As detailed in sect. **2**, since these spectra were acquired using the multibunch synchrotron radiation, the observed pump-induced effects are averaged over the time elapsed between consecutive laser pulses. Figure 1 shows Mo 3d and Te 4d core levels as a function of the applied laser fluence. The acquisition was performed in laser on/laser off sequences, to keep track of permanent changes in the spectra. For fluences below 0.4 mJ/cm^2, all observed pump-induced effects were completely reversible and consisted of: i) a rigid shift of the whole spectrum to lower binding energies; ii) a decrease in the Te/Mo intensity ratio; iii) the increase of background signal in the low energy side of the Mo 3$d_{5/2}$ peak. The latter effect is partially irreversible with fluences above 0.4 mJ/cm^2, with some residual intensity persisting after switching off the optical excitation. The energy position of this feature is compatible with the Mo 3$d_{5/2}$ peak of the 1T' phase [8,18], located 0.6 eV below the 2H component, as indicated by the arrows in fig. 1. Due to the small intensity of such 1T' component (2.5% with respect to its 2H counterpart, as derived from the fits), no clear 1T' signal is detected below the broader and less intense Mo 3$d_{3/2}$ and Te 4d doublet, although their slight broadening is compatible with the creation of chemically inequivalent components. In addition, the decrease of the
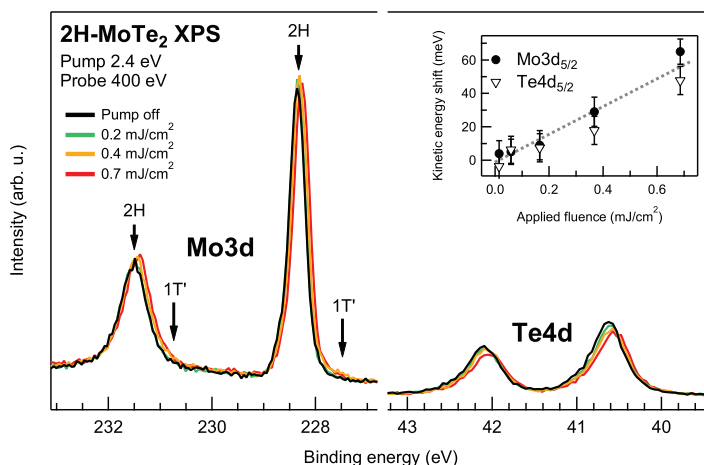

Fig. 1. – XPS spectra of Mo 3d and Te 4d regions as a function of the applied laser fluence. The spectra shift rigidly to lower binding energies due to surface photovoltage effects; as shown in the inset, the magnitude of the shift increases linearly with the applied laser fluence for both Mo 3d and Te 4d. The arrows indicate the position of Mo 3d peaks for 2H and 1T' phases. Photon energies of pump and probe were 2.4 eV and 400 eV, respectively. Reproduced from ref. [19] with permission from the Royal Society of Chemistry.
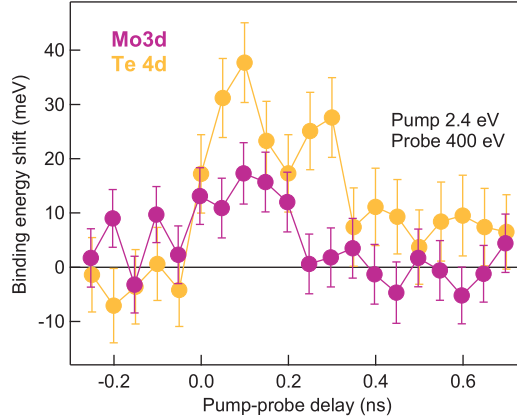
Fig. 2. – Mo $3d$ (purple) and Te $4d$ (orange) binding energy shifts as a function of the pump-probe delay. Photon energies of pump and probe were 2.4 eV and 400 eV, respectively, and the pump fluence was 0.7 mJ/cm^2.

Te/Mo intensity ratio ii) may also suggest a partial $2H$-to-$1T'$, since the $1T'$ phase is also characterized by Te vacancies [8, 18], whose diffusion and ordering is one of the proposed phase transition mechanisms [12, 20].

The spectral shift to lower binding energies i) is instead due to the surface photovoltage arising after exciton separation, indicating that the material behaves like a p-type semiconductor. The photovoltage shift magnitude increases linearly with the applied fluence (in the range probed), as shown in the inset of fig. 1. As stated above, these measurements are used to characterize the photoexcited system in the microsecond range. Instead, the main effect at short timescales is a rigid spectral shift to higher binding energies, as opposed to the photovoltage shift towards lower binding energies.

In fig. 2 the magnitude of the shifts obtained by fitting both Mo $3d$ and Te $4d$ peaks are reported as a function of the delay between pump and probe pulses. Before proceeding with further analyses of such data, however, it is worth summarizing the results presented so far, to clarify the differences between the acquisition modes used. In fig. 3 a scheme with the three cases is reported. The XPS spectrum recorded without optical excitation (a) is used for calibrating the binding energy position of the core levels in the ground state. The spectra recorded while illuminating the crystal without synchronizing the laser to the synchrotron (b) show the photo-induced effects averaged over 2.6 μs, the separation between two consecutive laser pulses. The net effect is a shift to lower binding energies due to SPV. Finally, the actual time-resolved scans are performed by synchronizing the pump to the hybrid pulses of Elettra (c). Interestingly, at short delay times a shift to higher binding energies is observed, which is opposed to the SPV shift. This fact seems to suggest that the two effects have different origins.

The Te $4d_{5/2}$ dynamics for a probe photon energy of 150 eV and an applied fluence of 0.7 mJ/cm^2 are reported with more detail in fig. 4. Unpumped (blue trace) and pumped spectra (red trace) are shown in the top graph of fig. 4(a). A rigid shift of the Te $4d_{5/2}$ line to higher binding energies, with respect to the position of the unpumped spectrum, is observed. The bottom graph of fig. 4(a) is a false color map reporting the difference between the pumped and unpumped signal as a function of the pump-probe delay, showing the persistence of the Te $4d_{5/2}$ line shift for several hundreds of
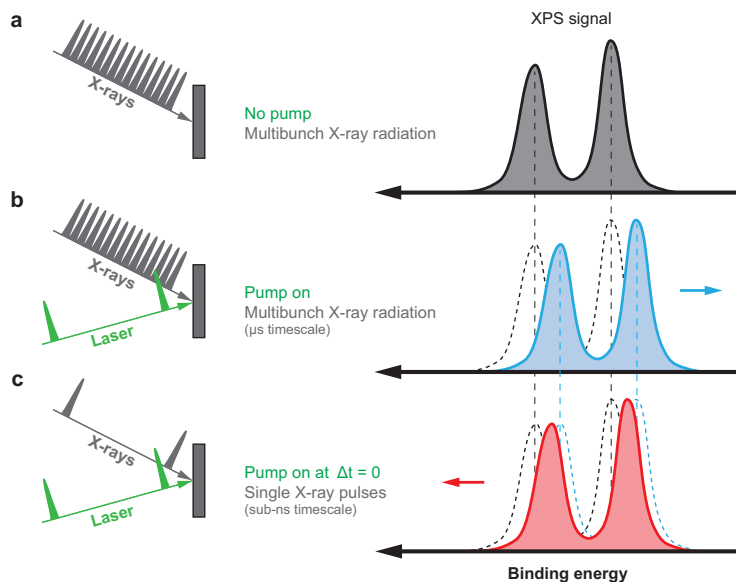
Fig. 3. – Scheme of the different acquisition modes. (a) The reference spectra are acquired without optical excitation to measure the reference binding energy of all components. (b) Using multibunch radiation as a probe while exciting the sample with the laser, the long-lived pump-induced modifications in MoTe$_2$ are detected. As indicated by the blue arrow, the main effect in a photovoltage shift to lower binding energies. (c) Time-resolved XPS measurements in the sub-nanosecond range require synchronized, single X-ray pulses as a probe. In this case a spectral shift to higher binding energy is observed. Reproduced from ref. [19] with permission from the Royal Society of Chemistry.

picoseconds. Figure 4(b) shows the magnitude of the binding energy shift (circles) as a function of the pump-probe delay, obtained from the fits. The time constant of the shift relaxation has been derived by fitting the data with an exponentially modified Gaussian (black trace), with the Gaussian full width at half maximum (FWHM) constrained to 120 ps to account for the instrumental response function, which is the cross-correlation between pump and probe pulses (green trace). A time constant $\tau = 580 \pm 120$ ps is found for the exponential decay.

The origin of the binding energy shift must be different than the SPV, as a in that case the shift direction should coincide with the one measured at longer delays [21-23]. Vacuum space-charge effects are also excluded, because the secondary electrons emitted by the pump were negligible, and because their usual fingerprint is a shift towards higher kinetic energies [24, 25]. Based on the timescale of the shift, lattice effects are a possible cause. A recent ultrafast electron diffraction study has revealed the coupling of hot carriers to high-energy phonons, causing lattice deformations [13]; lattice heating effects in the 100 ps range have also been detected by transient X-ray absorption spectroscopy [9, 10], and lattice cooling time constants of ∼200 ps have been observed in transient optical absorption [11].

Density functional theory (DFT) calculations have been used to examine whether changes in the chemical environment of the Te $4d$ electrons due to the distortion of the lattice could result in relevant shifts of the photoemission peak. In metals, the thermally
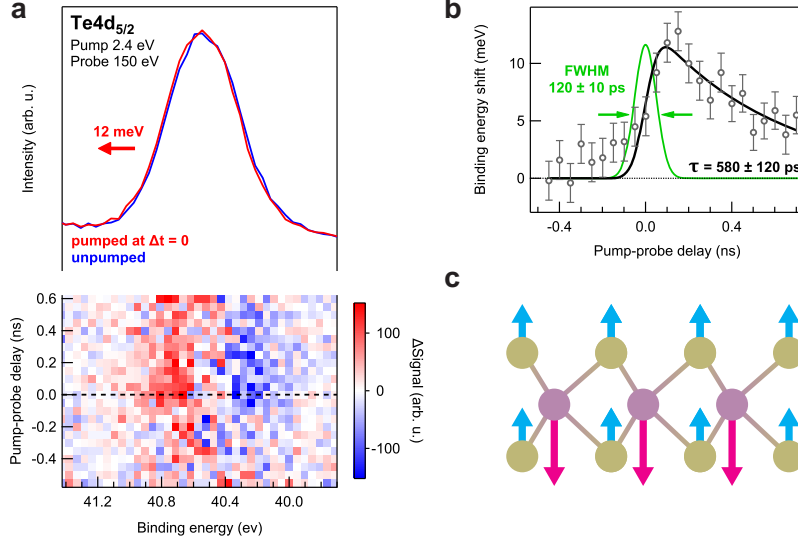
Fig. 4. – Time-resolved XPS measurements on the Te $4d_{5/2}$ line. (a) Unpumped (blue trace) and pumped (red trace) spectra at time zero reveal a rigid shift to higher binding energies. The false color map shows the difference between pumped and unpumped signal as a function of the pump-probe delay, highlighting the shift of the center of mass of the peak after photoexcitation. Photon energies of pump and probe were 2.4 eV and 150 eV, respectively, and the applied fluence was 0.7 mJ/cm². (b) Binding energy shift (circles) as a function of the pump-probe delay. An exponentially modified Gaussian (black line) was used to fit the data, yielding a time constant of 580±120 ps. The Gaussian full width at half maximum was constrained to 120 ps to account for the pump-probe cross-correlation (green trace). (c) Sketch of the A_2''-like displacements applied in the MoTe₂ layer to simulate the chemical shift observed experimentally. Purple: Mo; gold: Te. Reproduced from ref. [19] with permission from the Royal Society of Chemistry.

induced lattice expansion is known to cause binding energy shifts up to 30 meV increase in the Ta $4f$ binding energy [26]. In this case, a displacement of Mo and Te atoms in opposite directions along the c axis was used, to mimic the A_2'' phononic mode (see fig. 4(c)), since it is the dominant mode for photoexcitation at 2.4 eV [14]. More details on the DFT calculations are reported in ref. [19], while the results are summarized in table I. It emerges that the calculated binding energy difference (ΔE_B) of the Te $4d$ line increases linearly with the atomic displacement, with respect to the ground state, initially optimized positions. Such model agrees well with the experimental findings, and shows that a structural distortion of the MoTe₂ lattice can indeed cause the Te $4d$ level to shift for several meVs. From a linear extrapolation, it can be deduced that a ∼0.01 Å shift of the Mo atoms is sufficient to reproduce the ∼10 meV shift seen in fig. 4.

These results illustrate the possibility of extracting structural information from time-resolved X-ray photoemission spectra. Indeed, one of the main issues with time-resolved spectroscopies is the low initial excitation density, which determines the signal-to-noise ratio, but collective responses such as lattice heating, or the insurgence of SPV, result in the modification of the entire photoemission line, thus producing clearer photo-induced features [27]. In this case, assuming a reflectivity R = 0.44 (at normal incidence) and a penetration depth of 2×10^{-4} cm for MoTe₂ [28], and assuming one excited electron per absorbed photon, an upper limit of 5×10^{18} cm⁻³ is found for the excited carrier density

TABLE I. – *Mo and Te displacements along the c-axis and relative binding energy variations* (ΔE_B) *compared to the unperturbed initially optimized case. Reproduced from ref. [19] with permission from the Royal Society of Chemistry.*

Displacements along c-axis (Å)		
Mo	Te	ΔE_B (eV)
−0.025	+0.0125	0.03
−0.05	+0.025	0.06
−0.10	+0.05	0.11
−0.15	+0.075	0.14

with 0.7 mJ/cm^2 of applied fluence. This limit can be raised up to 1×10^{19} cm^{-3} by taking the quantum yield of 1.5-2 that has been observed in MoTe$_2$ [29] into account. By comparing this value to the electronic density of 2H-MoTe$_2$, that is, 18 valence electrons in a unit cell of 1.7×10^{-22} cm^3, a maximum excitation density of 0.01% is obtained. Photoemission signal coming from such a small percentage of excited centers would be buried in the background due to the unperturbed atoms, but the heating of the lattice, and the related atomic displacement, results in clear shifts of the core level lines in the 100 ps timescale.

4. – Conclusions

The photo-induced dynamics of 2H-MoTe$_2$ have been investigated by time-resolved X-ray photoemission spectroscopy. In the microsecond timescale, a surface photovoltage shift to lower binding energies is observed, which is compatible with the semiconducting nature of the crystal. At shorter timescales, core level shifts to higher binding energies are detected instead; the latter were ascribed to transient lattice deformations, with atomic displacements in the order of 0.01 Å estimated by DFT calculations. These results show that time-resolved X-ray photoemission, combined with theoretical simulations, can provide novel insights on the structural dynamics in layered materials, which are interesting not only from a fundamental perspective, but also for the possible exploitation of these materials in future optoelectronic devices.

* * *

REFERENCES

[1] MUNSON K. T., KENNEHAN E. R. and ASBURY J. B., *J. Mater. Chem. C*, **7** (2019) 5889.

[2] LAN C., SHI Z., CAO R., LI C. and ZHANG H., *Nanoscale*, **12** (2020) 11784.

[3] WANG X., CUI Y., LI T., LEI M., LI J. and WEI Z., *Adv. Opt. Mater.*, **7** (2019) 1801274.

[4] WANG Q. H., KALANTAR-ZADEH K., KIS A., COLEMAN J. N. and STRANO M. S., *Nat. Nanotechnol.*, **7** (2012) 699.

[5] ZHENG W., BONN M. and WANG H. I., *Nano Lett.*, **20** (2020) 5807.

[6] KRISHNAMOORTHY A., BASSMAN L., KALIA R. K., NAKANO A., SHIMOJO F. and VASHISHTA P., *Nanoscale*, **10** (2018) 2742.

[7] KOLOBOV A. V., FONS P. and TOMINAGA J., *Phys. Rev. B*, **94** (2016) 094114.

[8] CHO S., KIM S., KIM J. H., ZHAO J., SEOK J., KEUM D. H., BAIK J., CHOE D.-H., CHANG K. J., SUENAGA K., KIM S. W., LEE Y. H. and YANG H., *Science*, **349** (349) 625.

[9] BRITZ A., ATTAR A. R., ZHANG X., CHANG H.-T., NYBY C., KRISHNAMOORTHY A., PARK S. H., KWON S., KIM M., NORDLUND D., SAINIO S., HEINZ T. F., LEONE S. R., LINDENBERG A. M., NAKANO A., AJAYAN P., VASHISHTA P., FRITZ D., LIN M.-F. and BERGMANN U., *Struct. Dyn.*, **8** (2021) 014501.

[10] ATTAR A. R., CHANG H.-T., BRITZ A., ZHANG X., LIN M.-F., KRISHNAMOORTHY A., LINKER T., FRITZ D., NEUMARK D. M., KALIA R. K., NAKANO A., AJAYAN P., VASHISHTA P., BERGMANN U. and LEONE S. R., *ACS Nano*, **14** (2020) 15829.

[11] CHI Z., CHEN H., ZHAO Q. and WENG Y.-X., *J. Chem. Phys.*, **151** (2019) 114704.

[12] WANG Z., LI X., ZHANG G., LUO Y. and JIANG J., *ACS Appl. Mater. Interfaces*, **9** (2017) 23309.

[13] KRISHNAMOORTHY A., LIN M. F., ZHANG X., WENINGER C., MA R., BRITZ A., TIWARY C. S., KOCHAT V., APTE A., YANG J., PARK S., LI R., SHEN X., WANG X., KALIA R., NAKANO A., SHIMOJO F., FRITZ D., BERGMANN U., AJAYAN P. and VASHISHTA P., *Nano Lett.*, **19** (2019) 4981.

[14] PENG B., ZHANG H., W. CHEN W., B. HOU B., QIU Z.-J., SHAO H., ZHU,H., MONSERRAT,B., FU D., WENG H. and SOUKOULIS C. M., *npj 2D Mater. Appl.*, **4** (2020) 14.

[15] COSTANTINI R., STREDANSKY M., CVETKO D., KLADNIK G., VERDINI A., SIGALOTTI P., CILENTO F., SALVADOR F., DE LUISA, A., BENEDETTI D., FLOREANO L., MORGANTE A., COSSARO A. and DELL'ANGELA M., *J. Electron Spectros. Relat. Phenom.*, **229** (2018) 7.

[16] COSTANTINI R., GRAZIOLI C., COSSARO A., FLOREANO L., MORGANTE A. and DELL'ANGELA M., *J. Phys. Chem. C*, **124** (2020) 26603.

[17] COSTANTINI R., FABER R., COSSARO A., FLOREANO L., VERDINI A., HÄTTIG C., MORGANTE A., CORIANI S. and DELL'ANGELA M., *Commun. Phys.*, **2** (2019) 56.

[18] TAN Y., LUO F., ZHU M., XU X., YE Y., LI B., WANG G., LUO W., ZHENG X., WU N., YU Y., QIN S. and ZHANG X.-A., *Nanoscale*, **10** (2018) 19964.

[19] COSTANTINI R., CILENTO F., SALVADOR F., MORGANTE A., GIORGI G., PALUMMO M. and DELL'ANGELA M., *Faraday Discuss.*, **236** (2022) 429.

[20] SI C., CHOE D., XIE W., WANG H., SUN Z., BANG J. and ZHANG S., *Nano Lett.*, **19** (2019) 3612.

[21] TOKUDOMI S., AZUMA J., TAKAHASHI K. and KAMADA M., *J. Phys. Soc. Jpn.*, **77** (2008) 014711.

[22] BRÖCKER D., GIESSEL T. and WIDDRA W., *Chem. Phys.*, **299** (2004) 247.

[23] SHAVORSKIY A., NEPPL S., SLAUGHTER D. S., CRYAN J. P., SIEFERMANN K. R., WEISE F., LIN M.-F., BACELLAR C., ZIEMKIEWICZ M. P., ZEGKINOGLOU I., FRAUND M. W., KHURMI C., HERTLEIN M. P., WRIGHT T. W., HUSE N., SCHOENLEIN R. W., TYLISZCZAK T., COSLOVICH G., ROBINSON J., KAINDL R. A., RUDE B. S., ÖLSNER A., M'AHL S., BLUHM H. and GESSNER O., *Rev. Sci. Instrum.*, **85** (2014) 093102.

[24] HELLMANN S., ROSSNAGEL K., MARCZYNSKI-BÜHLOW M. and KIPP L., *Phys. Rev. B*, **79** (2009) 035402.

[25] Dell'Angela M., Anniyev T., Beye M., Coffee R., Föhlisch A., Gladh J., Kaya S., Katayama T., Krupin O., Nilsson A., Nordlund D., Schlotter W. F., Sellberg J. A., Sorgenfrei F., Turner J. J., Öström H., Ogasawara H., Wolf M. and Wurth W., *Struct. Dyn.*, **2** (2015) 025101.

[26] Riffe D., Hale W., Kim B. and Erskine J., *Phys. Rev. B*, **54** (1996) 17118.

[27] Costantini R., Morgante A. and Dell'Angela M., *J. Electron Spectros. Relat. Phenom.*, **254** (2022) 147141.

[28] Beal A. R. and Hughes H. P., *J. Phys. C: Solid State Phys.*, **12** (1979) 881.

[29] Kim J.-H., Bergren M. R., Park J. C., Adhikari S., Lorke M., Frauenheim T., Choe D.-H., Kim B., Choi H., Gregorkiewicz T. and Lee Y. H., *Nat. Commun.*, **10** (2019) 5488.